Journal of the European Ceramic Society 17 (1997) 1741–1748

PII: S0955-2219(97)00035-6
0955-2219/97/$17.00

Electrical and Optical Properties of Magnetron-Sputtered Y_2O_3 Stabilized ZrO_2 Thin Films

M. Boulouz,[a] F. Tcheliebou[b] & A. Boyer[a]*

[a]Centre d'Electronique et de Micro-Optoélectronique de Montpellier, Université Montpellier II, Place Eugène Bataillon, case 075, 34095 Montpellier cédex 5, France
[b]Department of Materials Science and Engineering, Pohang University of Science and Technology, San 31, Hyoja, Pohang, 790–784, Republic of Korea

(Received 13 September 1996; accepted 10 February 1997)

Abstract

The frequency dependence of both the ac conductivity and dielectric constant of thin films of ZrO_2-Y_2O_3 deposited on nickel substrates have been investigated in the frequency range 10 KHz to 10 MHz. It is shown that the total ac *conductivity, $\sigma(\omega)$, obeys the equation $\sigma(\omega) = A\omega^s$. The frequency and temperature dependences of the parameter* 's' *are reported and analyzed. It appears that for ZrO_2 and ZrO_2-Y_2O_3 films, the conduction mechanism is thermally activated and both the overlap large polaron tunnelling and the correlated barrier-hopping of charge carrier over localized states fit the experimental data, depending on the Y_2O_3 content. The dielectric constant, (ϵ), lies in the range 22 to 38 at room temperature and decreases with increasing frequency. The sample containing 8 wt% Y_2O_3 displays the largest dielectric constant of 38. The loss tangent is found to be in the order of 10^{-3}. The refractive index shows some dispersion and a maximum value of 2·19 for the ZrO_2–8 wt% Y_2O_3 at the wavelength of 760 nm. The extinction coefficient in the order of 10^{-3} is reported in the visible spectrum, which makes the films useful for some optical applications.* © *1997 Elsevier Science Limited.*

Resumé

Nous avons étudié la conductivité électrique en regime alternatif ($\sigma_{ac}(\omega)$), et la constante diélectrique (ε) des couches minces de ZrO_2 et de ZrO_2 stabilisée Y_2O_3 déposées sur des substrats de nickel, dans la gamme de fréquence allant de 10 kHz à 10 MHz, et pour des températures comprises entre 27 et 450°C. Nous avons observé que la conductivité totale obéit à l'équation $\sigma_{tot}(\omega) = A\omega^s$. Il apparaît que pour tous les films étudiées, la conductivité électrique est thermiquement activée. Les données expérimentales s'accordent soit sur le modèle de conduction par effet tunnel du polaron, soit sur celui du saut correlé des charges au-dessus des barrières séparant deux sites localisés voisins, en fonction de la concentration pondérale de Y_2O_3. La constante diélectrique varie entre 22 et 38 à la température ambiante et diminue avec une augmentation de la fréquence. L'échantillon dopé à 8% en poids de Y_2O_3 présente la constante diélectrique la plus élevée. La tangente de l'angle des pertes mesurée est de l'ordre de 10^{-3}. L'indice de réfraction présente une dispersion commune à la plupart des oxydes et une valeur optimale de 2·19 à la longueur d'onde de 750 nm et pour l'échantillon contenant 8% en poids de Y_2O_3. Dans l'ensemble, les dépôts présentent un coefficient d'extinction de l'ordre de 10^{-3} dans le spectre du visible.

1 Introduction

The diversified properties of zirconia have led to its use in a wide variety of device applications. It has been shown that the introduction of aliovalent cation in pure ZrO_2 lattice results in the creation of oxygen vacancy to preserve local charge balance. The defects are known to be very mobile and responsible for rapid ionic conduction in stabilized ZrO_2.[1] One prominent use of ZrO_2-based solid electrolytes is the oxygen sensor device. For most transition metal oxides, the dispersion of *ac* conductivity follows the equation $\sigma_{ac}(\omega) = A\omega^s$, where the frequency exponent '*s*' is less than unity. The identification of the conduction mechanism is based on both the frequency and temperature dependence of $\sigma_{ac}(\omega)$ and *s*. Abelard and Baumard[2]

*To whom correspondence should be addressed.

reported on the electrical properties of ZrO_2-Y_2O_3 single crystals in the frequency range 1·6 Hz–100 kHz. They attributed the frequency dispersion of σ_{ac} to the interactions between mobile oxygen vacancies and randomly distributed frozen-in yttrium dopant ions. Badwal[3] reported on the electrical conductivity in polycrystalline Y_2O_3-ZrO_2 in bulk form. Several other reports on the electrical and dielectric behaviour of ZrO_2 stabilized with various oxides are available in the literature,[4,5] mostly for single crystal and polycrystalline bulk materials. Moreover, the interpretation of collected experimental data is very often contradictory. Tcheliebou *et al.*[6] have recently investigated the *ac* conductivity and dielectric properties of polycrystalline ZrO_2 thin films stabilized with MgO, CeO_2, and Gd_2O_3 by electron-beam evaporation. It was found that the electrical conductivity is thermally activated and dominated by the correlated barrier hopping of charge carriers. J. D. Solier *et al.*[7] have measured the ionic conductivity of rf-sputtered yttria stabilized zirconia. The authors reported the values of about 3×10^{-6} and 2×10^{-14} $\Omega^{-1}cm^{-1}$ for temperatures of 350 and 25°C respectively. These values of ionic conductivity were very small compared to the conductivity measured in our work for the same range of temperature. Consequently, we neglected the contribution of σ_{ionic}, the electrical conductivity measured is mainly electronic.

Zirconium dioxide has attracted great interest concerning its use in optical coatings for systems operating in harsh environments, such as mirrors for lasers, as a high laser damage threshold can be achieved using this material. It has been emphasized elsewhere that the properties of thin films depend to some extent upon the deposition technique. In a previous work, we reported on the structural properties of polycrystalline Y_2O_3 stabilized ZrO_2 films obtained by the reactive thermal evaporation technique using an electron gun.[8] The crystallographic structure was found to change from a mixture of monoclinic and tetragonal phase for pure zirconia, to a single cubic phase for the 16 wt% Y_2O_3 composition. We have implemented recently a planar magnetron-sputtering system for thin films fabrication. Although the deposition rate is low compared with the electron beam apparatus, improvement in film quality is expected.

The pure zirconia films show diffraction peaks corresponding to the monoclinic phase. The layers containing 8 wt% Y_2O_3 exhibit a mixture of monoclinic and cubic phases, but cubic phase is predominant. As the weight percentage of Y_2O_3 increases, the mixture of the monoclinic and cubic phases disappears to the benefit of the single cubic phase. Fully stabilized zirconia in cubic phase appeared for the samples containing 15 and 20 wt% Y_2O_3. The surface morphology micrographs are obtained with scanning electron microscopy; all the films show dense columnar structure with smooth surfaces.

The objective of this work is to optimize the optical constants of ZrO_2 thin films for a certain wavelength or a wavelength range. Before that, however, we report the results of our basic research on the electrical properties including *ac* conductivity, dielectric constant, and loss tangent of pure ZrO_2 and Y_2O_3 stabilized ZrO_2 films obtained by magnetron-sputtering.

2 Theoretical discussions

2.1 On the interpretation of *ac* conductivity

Different theoretical explanations for the *ac* conduction in dielectric materials which contain both amorphous as well as crystalline phase have been developed to explain the frequency and temperature dependence of σ_{ac} and s. It is commonly believed that the pair approximation[9] holds, namely, the dielectric loss occurs because the carrier motion is considered to be localized within a pair of sites. Two fundamental mechanisms which have been developed are (1) the quantum-mechanical tunnelling (QMT) through the barrier separating two equilibrium positions[10] and (2) the hopping of a carrier over the barrier.[11,12]

According to the QMT model, the expression for the ac conductivity can be written as:

$$\sigma_{ac}(\omega) = Ce^2k_BT\alpha - 1[N(E_f)]^2\omega R(\omega)^4 \qquad (1)$$

where C is a numerical constant that may be taken as $\pi^4/24$, α a is the wave-function decay constant such that $\exp(-2\alpha R)$ represents an electron overlap integral between nearest-neighbor sites, $N(E_f)$ is the density of state at the Fermi level, and R is the hopping distance at frequency ω, given by:

$$R_\omega = \frac{1}{2\alpha} ln \frac{1}{\omega\tau_0} \qquad (2)$$

where τ_0 is the characteristic relaxation time. The frequency exponent in this model takes the form:

$$S = 1 + \frac{4}{\ln(\omega\tau_0)} \qquad (3)$$

Therefore the QMT model predicts a linear temperature dependence of $\sigma ac(\omega)$, but s is temperature-independent and frequency-dependent; s should decrease with an increase in frequency.

Long[13] has discussed the case where an appreciable overlap of the polaron-hopping distortion cloud occurs (OLPT) thereby reducing the value of the polaron hopping energy. In this case the ac conductivity σ_{ac} is shown to be of the form:

$$\alpha_{ac} = \frac{\pi^4}{12} e^2 (k_B T)^2 [N(E_f)]^2 \chi \quad \text{where} \quad \chi = \frac{\omega R^2}{2\sigma k_B T + W_{HO}\gamma_p / R^2}, \tag{4}$$

$W_{HO} = e^2/\varepsilon_p r_p$, ε_p and r_p are the effective dielectric constant and polaron radius respectively. The exponent s in the OLPT model is calculated to be:

$$S = 1 - \frac{8\alpha R + 6\beta W_{HO} r_p / R}{(2\alpha R + \beta W_{HO} r_p / R)^2} \tag{5}$$

where $\beta = 1/k_B$T. In this model, s should be both temperature-and frequency-dependent. The frequency exponent s is predicted to decrease from unity with increase in temperature.

The CBH model, which correlates the barrier W with the intersite separation R was proposed by Pike[11] for single electron hopping and further extended by Elliot[12] for the two electrons hopping simultaneously. The *ac* conductivity in the CBH model has the following expression:

$$\sigma_{ac} = \frac{\pi^3}{24} N^2 k_B T \varepsilon_0 \varepsilon w R(\omega)^6 \tag{6}$$

where N is the concentration of the localized states. The frequency exponent s is evaluated as:

$$S = 1 - \frac{6k_B T}{W_M + k_B T \ln(\omega\tau_0).} \tag{7}$$

Therefore, a temperature-dependent frequency exponent s is predicted, with s increasing towards unity as $T \Rightarrow 0$.

2.2 On the Tomlin's approach of determination of thin films optical constants

The optical constants of a thin film deposited onto a thick substrate can be determined from the measurements at normal incidence of the reflectance of the light on the film surface, R, and its transmittance, T, through the film. Let us consider light of wavelength λ in a non-absorbing medium of refractive index n_0 incident normally on a film of thickness d and complex refractive index $n_1 - ik_1$ which is supported on a substrate of complex refractive index $n_2 - ik_2$. According to Tomlin,[14] R and T are related to the film and substrate parameters by:[15]

$$\begin{aligned}\frac{1+R}{T} = \frac{1}{4n_0 n_2 (n_1^2 + k_1^2)} [&(n_0^2 + n_1^2 + k_1^2) \\ &x\{(n_1^2 + n_2^2 + k_1^2 + k_2^2)\cos h2\alpha_1 + \\ &2(n_1 n_2 + k_1 k_2)\sin h2\alpha_1\} + (n_0^2 - n_1^2 - k_1^2) \\ &x\{(n_1^2 - n_2^2 + k_1^2 + k_2^2)\cos h2\gamma_1 + \\ &2(n_1 k_2 - n_2 k_1)\sinh 2\gamma_1\}]\end{aligned} \tag{8}$$

and

$$\begin{aligned}\frac{1-R}{T} = \frac{1}{2n_2 (n_1^2 + k_1^2)} [&n_1\{(n_1^2 + n_2^2 + k_1^2 + k_2^2) \\ &\sin h2\alpha_1 + 2(n_1 n_2 - k_2 k_1)\cos h2\alpha_1\} \\ &+ k_1\{(n_1^2 - n_2^2 + k_1^2 - k_2^2)\sin 2\gamma_1 \\ &- 2(n_1 k_2 n_2 k_1)\cos 2\gamma_1\}]\end{aligned} \tag{9}$$

where $\gamma_1 = 2\pi n_1 d/\lambda$; $\alpha_1 = 2\pi k_1 d/\lambda$; d is the film thickness. The major problem is the multiplicity of the solutions; measurement errors should be of consideration when selecting meaningful solutions.[16] In addition, by using the experimental data for R and T together with the complex refractive index of the substrate determined by ellipsometry, the solution can be obtained by a numerical method. An approximate value of d from profilometry measurements is helpful for evaluation.

3 Experimental procedures

The targets were disks of Zr (99·98%) of 51 mm diameter for the fabrication of pure ZrO_2, and of ZrO_2 stabilized with the nominal content of Y_2O_3 for the fabrication of ZrO_2-Y_2O_3 films. The vacuum chamber was evacuated using a turbomolecular pump to 10^{-6} mbar. High-purity mixed oxygen–argon introduced during deposition raised the pressure to $1{\cdot}3\times10^{-3}$ torr. Oxygen concentration in the sputtering gas was 10% and the sputtering power was 75 W. The target to substrate distance was 3·4 cm and was kept fixed for each deposition run. Prior to the deposition, the targetswere pre-sputtered for some few minutes to remove any contamination on its surface. The films were deposited on optically polished pyrex and nickel substrates of 10 mm in diameter, attached to a substrate holder. A heater mounted above the holder enables the temperature of the substrate to be varied from ambient to 600°C. A thermocouple (Chromel-Alumel) placed in contact

with the substrate was used to monitor the substrate temperature.

After deposition, sputtered nickel dot electrodes were made on the sample deposited on nickel using a radiofrequency diode-sputtering system, to make an MIM structure for electrical measurements. These were carried out in a vacuum chamber evacuated to approximately 10^{-3} torr. Both the electrical conductivity and permittivity were measured as a function of temperature (25°C–450°C) and frequency (10 kHz–10 MHz) by a capacitance bridge technique, with a Hewlett-Packard LCR meter 4275 A.

The measurements of transmittance (T), and reflectance (R), at normal incidence of the films deposited on pyrex substrate were performed in the wavelength range 350–800 nm using a UV Beckman 5240 spectrophotometer. The complex refractive index n-ik and film thickness were calculated from R and T following Tomlin's approach.[17] Film thickness was also determined by surface profilometry using a Talystep. Substrate optical constants were measured using a phase modulation ellipsometer and confirmed by the analysis of the substrate transmittance.

4 Results and discussion

4.1 Electrical properties

4.1.1. Frequency and temperature dependence of σ_{ac}

The frequency dependence of the total *ac* conductivity, $\sigma(\omega)$, for samples of different compositions is depicted in Fig. 1. At room temperature, for the overall samples, the plot is a straight line and follows the 'universal' law $\sigma_{tot}\,\sigma(\omega) = A\omega^s$, suggesting a distribution of relaxation times. This may arise from local disorder [Fig. 1(a)]. Figure 1(b) shows the typical frequency dependence of the electrical conductivity in the sample investigated. As the temperature increases, $\sigma(\omega)$ shows frequency-independent conductivity at low frequencies and the linear behaviour is shifted to high frequency. At approximately 10 kHz for the composition displaying high conductivities (8 wt% Y_2O_3 and 15 wt% Y_2O_3) the total conductivity is nearly constant and increases further with increasing frequency. The electrical conduction is thermally activated. At high temperatures, the total *ac* conductivity can be deconvoluted in two components σ_{dc} and $A\omega^s$ such as stot $\sigma_{tot}(\omega)$ follows the relation:

$$\sigma_{tot}(\omega) = \sigma_{dc} + A\omega^s \qquad (10)$$

where σ_{dc} is the frequency-independent component, and A is a constant independent of frequency. The exponent 's' of the angular frequency ω lies in the range $0 < s < 1$. It has been emphasized that when the same conduction process is responsible for the conduction, σ_{dc} is different from the limit of $\sigma_{tot}(\omega)$ when $\omega \Rightarrow 0$. Therefore the above equation is no longer valid.

The temperature-dependence of the electrical conductivity of the ZrO_2-Y_2O_3 thin films, measured in the 25–400°C, is shown in Fig. 1(c). The $\log[\sigma(\omega)]$ is plotted against $10^3\,T^{-1}$ for different concentrations. Pure ZrO_2 shows a nearly linear dependence on the temperature. For the samples containing Y_2O_3 additive, whatever the concentration, the plot shows a curvature at about 300°C, indicating a change in the activation energy, due to a gradual dissociation of oxygen vacancies — defects cations associates. At high temperatures, the conductivity is predominantly ionic and asso-

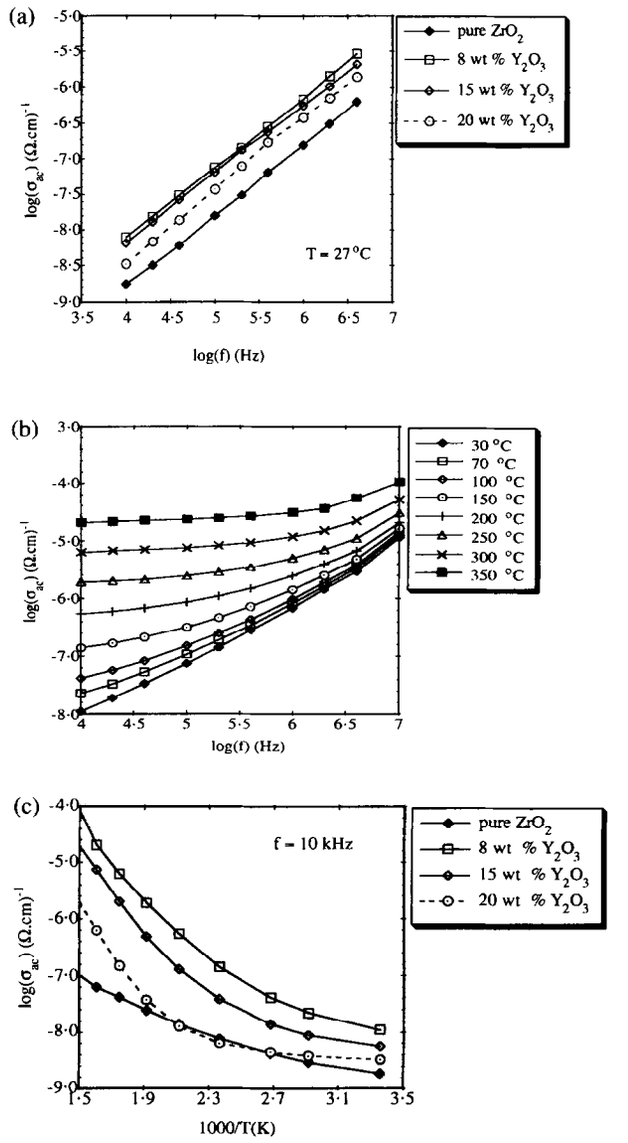

Fig. 1. (a) Frequency dependence of the total *ac* conductivity in ZrO_2-based films; (b) typical variation of the total conductivity with frequency measured at different temperatures, and (c) temperature dependence of the conductivity showing the change in the activation energy.

ciated with higher activation energies. In the low temperature region, the total conductivity is dominated by the electronic contribution (hopping over barriers between neighboring localized states). Similar variations of the conductivity have been reported in the literature.[18] In order to identify the conduction mechanism in these materials, the frequency exponent '*s*' is plotted as a function of both temperature and frequency. Figure 2(a) shows an increase in s with increasing frequency for the pure ZrO_2 and ZrO_2 stabilized with 8 wt% Y_2O_3 and 15 wt% Y_2O_3. Based on the discussion in Section 2, the increase in s with frequency is consistent with both the CBH model [eqn (7)] and the overlapping large polaron tunnelling (OLPT) for a reduced polaron radius model, developed by Long.[13] Fig. 2(b) shows the temperature dependence of s for different Y_2O_3 content. It can be seen that for all compositions, s increases with decreasing temperature. The OLPT model predicts an appreciably stronger temperature dependence of $\sigma_{ac}(\omega)$ in the temperature regime where the frequency exponent *s* is a decreasing function of temperature. According to the correlated barrier hopping (CBH) model, a temperature dependent *s* is predicted with *s* increasing towards unity as $T \Rightarrow 0$. This seems to be rigorously met in Figure 2(b) only for the sample containing 20 wt% Y_2O_3, but is in contrast with the simple hopping-over-the-barrier model. Therefore, the correlated barrier-hopping model is suitable for the interpretation of the data for ZrO_2–8 wt% Y_2O_3 and ZrO_2 — 15 wt% Y_2O_3. It is reasonable to state that the conduction mechanism in ZrO_2-Y_2O_3 is Y_2O_3 content dependent. Up to 15 wt% Y_2O_3, the CBH model describes the data fairly well whereas around 20 wt% Y_2O_3, the OLPT model is applicable to explain the ac conductivity data.

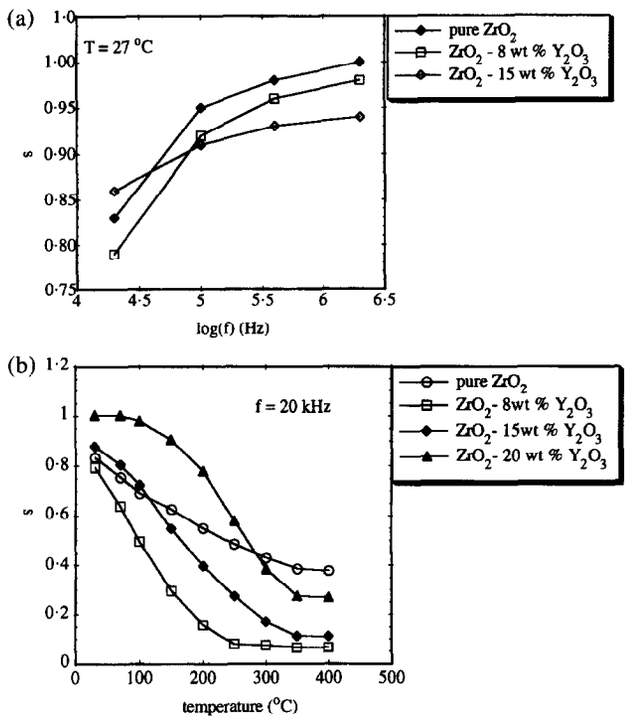

Fig. 2. (a) Frequency dependence of the frequency parameter 's' and, (b) its temperature dependence.

4.1.2. Effect of the Y_2O_3 content

Figure 3 shows the dependence of the *ac* electrical conductivity on the Y_2O_3 content in the ZrO_2 lattice. At room temperature the *ac* conductivity increases slightly from that of the pure zirconia to a nearly flat maximum in the range 10–15 wt% Y_2O_3 and decreases further. In the ZrO_2-based systems, it has been mentioned in nearly all reports that a maximum electrical conductivity appears at the minimum dopant concentration (wt% or mol%) required to stabilize the cubic phase. We have reported on such data recently on the CeO_2-ZrO_2, MgO-ZrO_2 and Gd_2O_3-ZrO_2 systems.[6] We believe that a probable explanation of the Y_2O_3 content dependence of σ_{ac} may be the following: addition of Y_2O_3 results in the formation of defects responsible for the ionic conductivity. The defect density increases with increasing dopant content up to 8 wt% Y_2O_3 where the ZrO_2 structure changes from a mixture of monoclinic and tetragonal to a cubic structure. Further Y_2O_3 addition results in an aggregation of vacancies and accordingly, a reduction in the conductivity occurs. It is worth pointing out that most of the data reported on stabilized ZrO_2 are interpreted in various ways and should therefore be viewed with some caution. The phase assemblage in these systems is complex and may consist of two or more phases in addition to variants of the same phase with different degrees of dopant distribution.[19] Moreover, the change in the conductivity behaviour with the dopant content at a constant temperature, and the conductivity behaviour as a function of temperature have been discussed in terms of varying degrees of interaction between defect pairs, ordering of vacancies and different defect configuration.[20]

4.1.3. Dielectric constant

Figure 4 shows the variation of dielectric constant (ε') and the loss tangent (tan δ) with frequency for different temperatures in the ZrO_2–8 wt% Y_2O_3 sample. For other compositions, the dispersion depicted in Fig. 4(a) is typical. At room temperature, ε' is nearly frequency-independent for the overall samples. The dispersion was found to be more marked at higher temperatures. The frequency response in the samples studied is consistent with the simple electrical model of a capacitance C_p in parallel with a resistance R_p if one neglects the electrode polarization. Therefore,

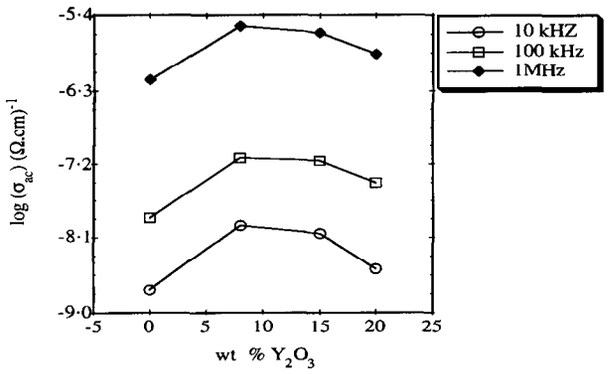

Fig. 3. Effect of Y_2O_3 content on the total electrical conductivity at various frequencies.

the real ε' and the imaginary ε'' parts of the dielectric constants are determined as:[21]

$$\varepsilon' = \varepsilon_\infty + \frac{\varepsilon_s - \varepsilon_\infty}{1 + \omega^2\tau^2} \tag{11}$$

and

$$\varepsilon'' = \frac{(\varepsilon_s - \varepsilon_\infty)\omega\tau}{1 + \omega^2\tau^2} \tag{12}$$

where $\tau = R_pC_p$ is the relaxation time: ε_s is the static dielectric constant whereas ε_∞ is the high frequency limit. In the model described above, the loss is given in terms of the loss tangent, defined as $\tan\delta = \varepsilon''/\varepsilon'$. The loss arises from the long range migration of charge carriers or the dissipation of the energy associated with the rotation or oscillation of dipoles.

Figure 4(b) shows the temperature-dependence of the real part of the dielectric constant ε'. At room temperature, the dielectric constant is shown to be constant. As the temperature is raised, the dielectric constant increases markedly; the dielectric relaxation strength $\varepsilon_s - \varepsilon_\infty$ becomes very important. Above 200°C, the rapid increase in ε' is associated with the presence of space charge polarization in the compounds. This is evidenced by the highest increase noticed at 10 kHz. At frequencies above 1 MHz, the space charge polarization is negligible. It should be mentioned that the electrode polarization contribution increases with increasing temperature and the simple model invoked can no longer be called for to interprete the frequency-dependence of the high temperature of the dielectric constant.

One can also see in Fig. 4(c) that in the frequency range considered, a maximum in ε' appears for the ZrO_2 – 8 wt.% Y_2O_3 sample. In a previous work, we have noticed that this corresponds to the minimum content for the stabilization of the cubic phase. Therefore, the optimum may be attributed to the change in the number of polarizable particles per unit cell during the phase transition to a cubic structure, through the well known Clausius–Mosotti relation:[21]

$$\frac{\varepsilon' - 1}{\varepsilon' + 2} = \frac{N\alpha}{3V\varepsilon_0} \tag{13}$$

where N is the number of polarizable particles per unit cell of volume V, α is its polarizability, and ε_0 the permittivity of the free space. The appearance of the cubic phase is accompanied with a shrinkage of the unit cell. In the frequency range 10^3 Hz–107 Hz, the dipolar polarization, which involves the perturbation of the thermal motion of ionic or molecular dipoles, shows the only frequency dependent contribution to the total polarization.

At room temperature and at the frequency of 1 MHz [Fig. 4(d)], tan δ is in the order of 0·015 for pure ZrO_2, 0·038 for ZrO_2–8 wt% Y_2O_3, which confirms that the real part of the permittivity is the largest contributor to the total dielectric constant. No peak of relaxation was evidenced in this work. However, the sharp increase in tan δ for frequencies above 1 MHz may predict a relaxation peak above 10 MHz.

4.2 Optical constants

4.2.1. Refractive index

Figure 5(a) shows the dispersion of the refractive index (n) for the pure ZrO_2 and the samples containing 8 wt% Y_2O_3, 15 wt% Y_2O_3; and 20 wt% Y_2O_3. For the overall films, the refractive index is relatively high and increases for shorter wavelengths. The strong increase of the refractive index at short wavelengths is associated with the band-gap absorption edge. Above 700 nm, only a slight variation of n with the wavelength is noticed. However, in the spectral range shown, the dispersion of n is very large (about 10%).

A careful examination of Fig. 5 shows also that for all the samples in the visible spectrum, ZrO_2–20 wt% Y_2O_3 displays the lowest refractive index. However, it can be seen that as Y_2O_3 is added to pure ZrO_2, the refractive index is raised up to a maximum of 2·19 at the wavelength of 760 nm, for the sample doped with 8 wt% Y_2O_3. Further increase in Y_2O_3 content in the mixture results in a decrease of the refractive index. We attribute this behaviour to the change in the crystallographic structure. The cubic phase, close packed, appears in the ZrO_2-Y_2O_3 system at about 8 wt% Y_2O_3. Above this concentration, additional Y_2O_3 gives rise to an increase in the volume of the unit cell. This is consistent with the increase in the lattice parameter variation reported previously.[8,22]

Feldman *et al.*[23] have noticed in the ZrO_2-SiO_2 system that a large admixture of SiO_2 yields films having an amorphous structure with high porosity. It may be reasonable to believe that the decrease in the refractive index is consistent with low packing density induced in the film during the stabilization process. Low packing density causes a decrease in film refractive index.

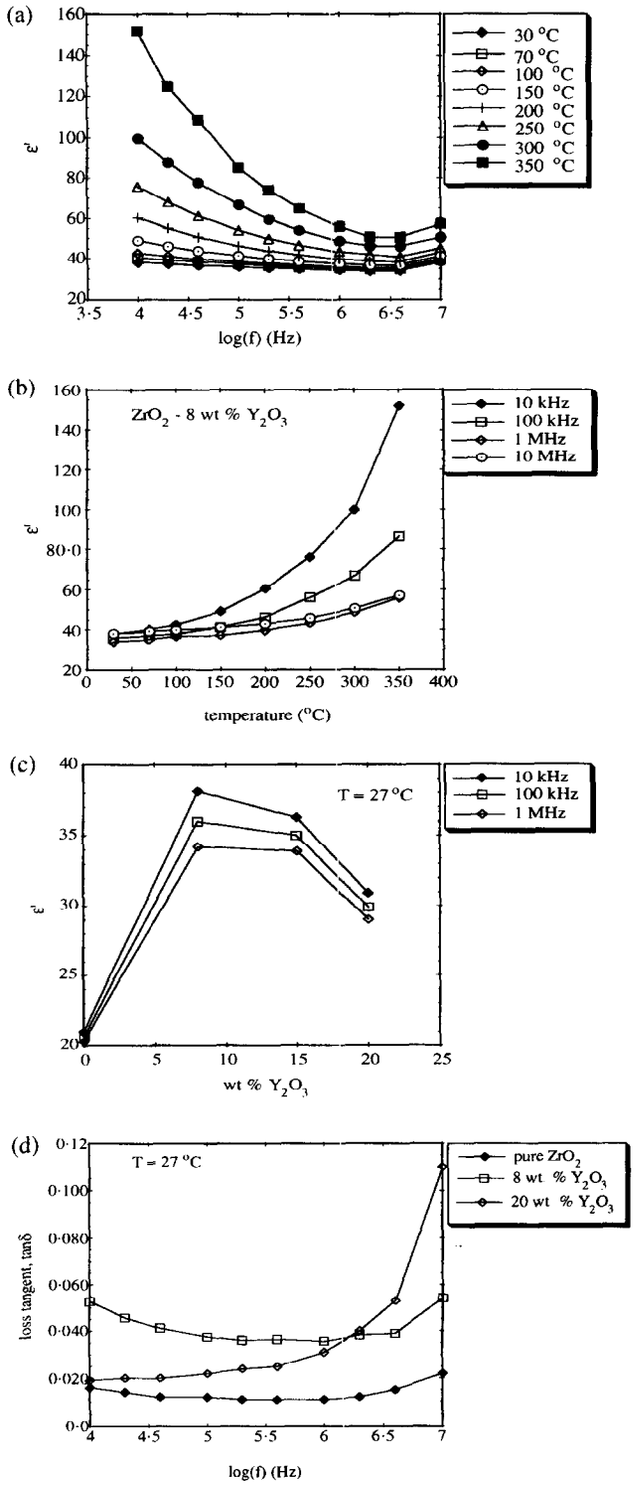

Fig. 4. (a) Dispersion of the real part of the dielectric constant, ε'; (b) temperature dependence of ε' at different frequencies; (c) effect of Y_2O_3 additive on the dielectric constant at room temperature; and (d) the variation of loss tangent withfrequency for different Y_2O_3 contents.

4.2.2. Extinction coefficient

The extinction coefficient (k) contributes to optical losses in thin optical coatings. Figure 5(b) shows that for the overall samples, the extinction coefficient is less than 0·009 above the wavelength of 400 nm. Unlike the refractive index, the extinction coefficient is nearly wavelength independent and increases gradually with the dopant content in the Y_2O_3-ZrO_2 system. During the stabilization of ZrO_2 with Y_2O_3, points defects are generated in the ZrO_2 matrix and their concentration increased with the Y_2O_3 content. Scattering is likely to occur in the bulk of the thin film and results in the variation of the extinction coefficient noticed in the present work. The values of the extinction coefficient reported here are higher than those published by Pulker[24] in pure zirconia thin films. The discrepancy may be explained by the uncertainty in the measurements as well as the pyrex substrates, the optical constants of which influence those of the ZrO_2-based thin films.

5 Conclusion

Electrical and optical properties of thin films of pure ZrO_2 and ZrO_2 stabilized with different amounts of Y_2O_3 deposited by *rf* magnetron sputtering have been investigated. The *ac* conductivity was studied in the frequency range 10 kHz–10 MHz for temperatures varying from room temperature to 450°C. It was found that for dopant content up

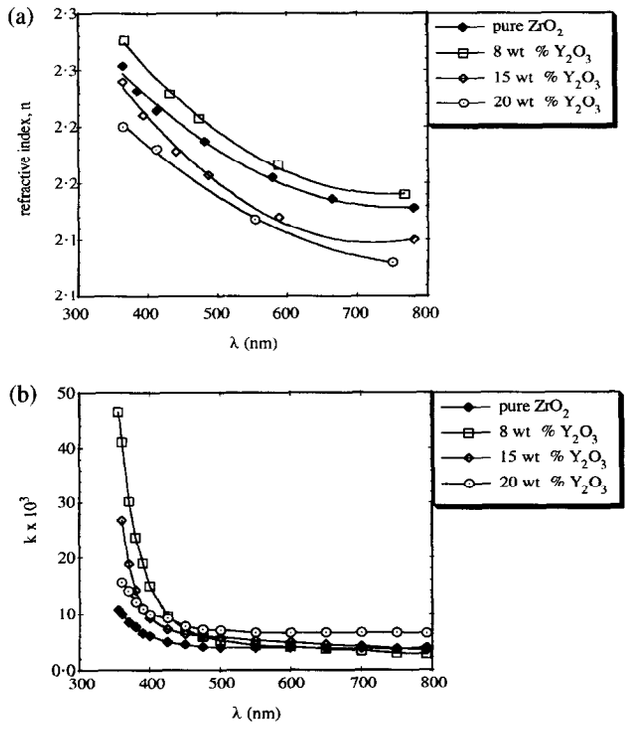

Fig. 5. (a) Dispersion of the refractive index for different compositions; and (b) variation of the extinction coefficient with wavelength in the visible spectrum.

to 15 wt% Y_2O_3, the correlated barrier-hopping model fitted the experimental data whereas, for the the sample containing 20 wt.% Y_2O_3, the overlap large polaron tunnelling (OLPT) was adequate for the explanation of both the temperature and the frequency-dependence of $\sigma_{ac}(\omega)$. Both the electrical conductivity and the dielectric constant showed a maximum for the 8 wt% Y_2O_3 sample, explained by crystallographic change according to the previous studies. The dielectric constant is found to be nearly frequency-independent at room temperature whilst the loss tangent is less than 0·06. The analysis of the optical transmission and reflection of the films deposited on pyrex substrates yielded a relatively high refractive index for the overall films in the visible spectrum and a high dispersion. At the wavelength of 760 nm, an optimum refractive index of 2·19 has been measured in the ZrO_2–8 wt% Y_2O_3. This optimum was ascribed to the high film density accompanying the appearance of the close packed cubic structure. In the visible range, all the films showed an extinction coefficient less than 0·009 in the visible spectrum. It was noticed that the structure of ZrO_2-based thin films markedly influences their electrical, dielectric and optical properties.

Acknowledgements

The authors are grateful to Mr L. Martin, Centre d'Electronique et de Micro-Optoélectronique de Montpellier for his assistance during the optical measurements. We are indebted to Harry and Frances Ashjean of RIST for reviewing this paper.

References

1. Etsell, T. H. and Flengas, S. N., The electrical properties of solid oxide electrolyte. *Chem. Rev.*, 1992, **70**, 339–352.
2. Abelard, P. and Baumard, J. F., Study of the *dc* and *ac* electrical properties of an yttria-stabilized zirconia single crystal $[(ZrO_2)^{0.88}$-$(Y_2O_3)^{0.12}]$. *Phys. Rev.*, 1982, **B26**, 1005–1017.
3. Badwal, S. P. S., Electrical conductivity of single crystal and polycrystalline yttria stabilized zirconia. *Journal of Mat. Sci.*, 1984, **19**, 1767–1776.
4. Muccillo, E. N. S. and Kleitz, M., Impedance spectroscopy of Mg-partially stabilized zirconia and cubic phase decomposition. *Journal of Eur. Ceram. Soc.*, 1996, **16**, 453–465.
5. Yamamoto, O., Arati, Y., Takeda, Y., Imanishi, N., Mizutani, Y., Kawai, M. and Nakamura, Y., Electrical conductivity of stabilized zirconia with ytterbia and scandia. *Solid State Ionics*, 1995, **79**, 137–142.
6. Tcheliebou, F., Boulouz, M. and Boyer, A., Electrical behaviour of thin ZrO_2 films containing some ceramic oxides. *Mat. Sci. Eng.*, 1996, **B38**, 90–95.
7. Solier, Juan de Dios, Pérez-Jubindo, Miguel A., Dominguez-Rodriguez, A. and Heuer, A. H., Low-temperature ionic conductivity of 9·4 mol%-yttria-stabilized zirconia single crystals. *Journal of Am. Ceram. Soc.*, 1989, **72**(8), 1500–1502.
8. Chéron, J. P., Tcheliebou, F. and Boyer, A., Structural properties of Y_2O_3 stabilized ZrO_2 films deposited by reactive thermal evaporation. *Journal of Vac. Sci. Technol.*, 1992, **A10**, 3207–3209.
9. Som, K. K. and Chandhuri, B. K., Electrical and dielectric properties of the $Bi_4Sr_3Ca_3Cu_4O_x$ (4:3:3:4) glassy semiconductor. *Phys. Rev.*, 1990, **B41**, 1581–1591.
10. Pollack, M. and Geballe, T. H., Low-frequency conductivity due to hopping processes in silicon. *Phys. Rev.*, 1961, **122**, 1742–1753.
11. Pike, G. E., Ac conductivity of scandium oxide and a newhopping model for conductivity. *Phys. Rev.*, 1972, **B6**, 1572–1780.
12. Elliott, S. R., Ac conduction in amorphous chalcogenide and pnictide semiconductors. *Advances in Physics*, 1987, **36**, 135–218.
13. Long, A. R.. *Advances in Physics*, 1982, **31**, 553.
14. Tomlin, S. G., Optical relection and transmission formulae for thin films. *Brt. Journal of Appl. Phys. (J. Phys. D)*, 1968, Ser.**2**, 1667–1671.
15. Denton, R. E., Campbell, R. D. and Tomlin, S. G., The determination of the optical constants of thin films from measurements of reflectance and transmittance at normal incidence. *Journal of Phys. D: Appl. Phys.*, 1972, **5**, 852–863.
16. Vignes, J., Algorithmes numériques. Analyse et mise en oeuvre. Vol. 2, ed Techni, Paris, 1980, p. 56.
17. Tomlin, S. G., More formulae relating to optical reflection and transmission by thin films. *Journal of Phys. D: Appl. Phys.*, 1972, **5**, 847–851.
18. Giuntini, J. C., Zanchetta, J. V. and Salam, F., Analysis of experimental problems connected with polarization conductivity measurements application to electronic and ionictransport. *Mat. Sci. Eng.*, 1995, **B33**, 75–84.
19. Badwal, S. P. S., Zirconia-based electrolytes: microstructure, stability and ionic conductivity. *Solid State Ionics*, 1992, **52**, 23–32.
20. Vilk, Yu N., Shvaiko, V. E., Shvaikovskii, and Shvarts, V. A., Non-stoichiometry in zirconia. *Refractories*, 1995, **36**, 247.
21. Hench, L. L. and West, J. K., *Principles of Electronic Ceramics*. John Wiley, Singapore, 1990, pp. 201-241
22. Tcheliebou, F., Studies on ZrO_2-based ceramics obtained by reactive thermal evaporation using an electron gun. Ph.D thesis, University of Montpellier II, Montpellier, 1995.
23. Feldman, A., Farabaugh, E. N. and Haller, W. K., Modifying structure and properties of optical films by coevaporation. *Journal of Vac Sci. Technol.*, 1986, **A4**, 2969.
24. Pulker, P. K., Optical losses in dielectric films. *Thin Solid Films*, 1976, **34**, 343–347.